Research Square

Preprints are preliminary reports that have not undergone peer review.
They should not be considered conclusive, used to inform clinical practice,
or referenced by the media as validated information.

Structural, Dielectric and Ferroelectric Properties of Lanthanum Doped PZT(52/48) Electroceramics

M. Prabu

mprabuaps@gmail.com

SRM Institute of Science and Technology

Habeeb Khan A. M.

Noorul Islam University

Research Article

Keywords: Ferroelectric, Relative permittivity, Impedance analysis, Activation Energy, Remnant Polarization, Coercive electricfield

Posted Date: May 4th, 2026

DOI: https://doi.org/10.21203/rs.3.rs-9126151/v1

License: This work is licensed under a Creative Commons Attribution 4.0 International License.
Read Full License

Additional Declarations: No competing interests reported.

Abstract

Technological advancement depends on the investigation of new materials and compositions that show a strong interaction between ferroelectric and piezoelectric capabilities. It has been demonstrated that lanthanum (La) doping improves lead zirconate titanate (PZT) ceramic performance in a number of ways. The conventional sol-gel process was used to produce a ceramic material with the composition $(Pb_{0.925}La_{0.075})(Zr_{0.52}Ti_{0.48})O_3$ in order to examine the impact of La inclusion on its ferroelectric and dielectric behaviour. The development of a pure perovskite phase with a tetragonal structure, devoid of any unwanted pyrochlore phase, was verified by X-ray diffraction (XRD). Thermogravimetric and differential thermal analyses (TGA/DTA) of the precursor gel indicated weight changes and thermal events associated with phase formation at elevated temperatures. Scanning electron microscopy (SEM) revealed uniformly distributed grains with an average size of approximately 300 nm in the sintered samples. Complex impedance spectroscopy (CIS) was used to assess the electrical characteristics at temperatures ranging from ambient temperature to 600°C and frequencies between 100 Hz and 1 MHz. The relative permittivity and dielectric loss both rose with frequency, according to the results, peaking at about 27,780 at 600°C. Based on the Arrhenius plot, the activation energy for DC conductivity was computed to be 0.169 eV. A coercive electric field (E_c) of 3.04 kV/cm and a remnant polarization (P_r) of 6.12 μC/cm² were obtained from ferroelectric experiments performed at room temperature with an applied voltage of 4000 V.

1. Introduction

Ferroelectric materials are being researched extensively because of their remarkable electro-optic, piezoelectric, pyroelectric, and dielectric characteristics. One of these, lead zirconate titanate (PZT), is notable for crystallizing in a perovskite structure (ABO_3). Due to their special properties, these ceramics can be used in a wide variety of applications, such as sensors, oscillators, charge storage devices, ferroelectric random-access memory (FRAM), transducers, and even some biomedical applications like anti-cancer therapies [1–4]. The ferroelectric performance of these materials is highly sensitive to both their composition and grain size, making microstructural engineering and doping strategies essential. PZT is particularly notable for its morphotropic phase boundary (MPB), which occurs when approximately 50–55% of titanium is replaced by zirconium in $PbTiO_3$. At this boundary, rhombohedral and tetragonal phases coexist, leading to enhanced dielectric and piezoelectric behaviour. These enhanced characteristics include a high relative permittivity, significant remnant polarization, and a low coercive electric field [5–7]. PZT ceramics are often mildly doped with various oxides to tailor their physical properties for specific applications. Lanthanum (La) is an important dopant that can further change the properties of the material since it can be introduced to the ABO_3 lattice as La^{3+} rather than Pb^{2+}. The ABO_3 structure has been doped with a variety of transition metal ions, including as La^{3+}, Mn^{2+}, Nb^{5+}, Zn^{2+}, etc., to enhance its ferroelectric and piezoelectric characteristics. The results indicated that this doping approach leads to notable changes in the material's physical properties, particularly in terms of saturation polarization, coercive field, and remnant polarization. Specifically, incorporating a

lanthanum-based compound into the $BaTiO_3$ perovskite lattice was found to enhance both the saturation magnetization and remnant polarization, with these effects becoming more pronounced at higher doping concentrations [8–12].

Lanthanum (La) modification is the most widely utilized technology for practical applications and has proven to be the most successful of the many attempts to improve the properties of these materials [13, 14]. La-modified PZT ceramics frequently have superior dielectric and piezoelectric properties compared to pure PZT because of the donor (softener) effect [5]. However, investigations using a Zr/Ti ratio of 52/48 for La doping in PZT are extremely rare [15, 16]. One of the most promising ferroelectric materials, both theoretically and practically, is lanthanum-doped lead zirconate titanate, especially for compositions close to the morphotropic phase boundary (MPB). It is ideal for usage in actuators, sensors, and memory devices due to its exceptional electromechanical performance and variety of physical properties. [13, 17]. It is well-established that introducing lanthanum into PZT tends to enhance relaxor-like behaviour. This effect is thought to stem from A-site vacancies created by La^{3+} substitution, which disrupt the long-range connectivity of ferroelectrically active octahedra and instead promote the formation of locally polarized regions [14, 18].

In this work, we used the sol-gel approach to synthesize PL(92.5/7.5)ZT(52/48) powder. A well-known and versatile chemical process called sol-gel synthesis makes it possible to synthesize nanoparticles, thereby establishing a new class of special materials. These materials' small particle size gives them a unique but superior morphology, and their crystallography and chemical composition are similar to those of their alloys created using more traditional methods, like solid-state reaction routes. Recent sol-gel research has led to the discovery of a method for crystallization in the colloidal form at relatively low temperatures (~ 100°C). This made it possible to create composite materials with mixed oxides, nanocrystalline oxides, and the low-temperature sol-gel process [19]. The synthesised material's phase composition and structural formation were confirmed using powder X-ray diffraction (XRD). The sample's thermal behaviour and crystallization process were also thoroughly examined utilizing thermogravimetric methods.

The sample's shape and particle size were investigated using scanning electron microscopy (SEM). At frequencies ranging from 100 Hz to 1 MHz, the temperature-dependent behaviour of the relative permittivity, loss tangent, and DC conductivity was assessed over a range of 25 to 600°C. The polarization-electric field (P-E) hysteresis loop of the PL(92.5/7.5)ZT(52/48) ceramic was analyzed to determine its remnant polarization (Pr) and coercive electric field (Ec). After then, the results were evaluated and subjected to critical analysis.

We doped PZT ceramics with lanthanum to enhance their ferroelectric and dielectric properties for application in MEMS-based devices. It has been demonstrated that lanthanum-doped PZT exhibits a higher relative permittivity and remnant polarization than undoped PZT [20]. However, despite the improved properties due to lanthanum doping, the Curie temperature is higher than that of undoped PZT.

This suggests that lanthanum-doped PZT is more suitable for applications involving all temperatures than its undoped counterpart.

2. Experimental Details

2.1. Materials

The following reagents were procured and utilized without further purification: lanthanum (III) nitrate hexahydrate (Alfa Aesar, 99.9%), lead (II) nitrate (Merck, 99.0%), citric acid monohydrate (Merck, 99.5%), titanium tetra-isopropoxide (Merck, 98%), zirconium oxychloride (Thomas Baker, 98.0%), and polyvinyl alcohol (PVA, Fischer, molecular weight: 125,000). Distilled and deionized water was obtained using a Milli-Q purification system (Millipore Milli Q185 Plus System, USA).

2.2. Methods

The synthesis procedure for PZT (52/48) ceramics was detailed in our earlier work [21]. In this study, the PLZT polycrystalline sample was prepared using the sol-gel method. Initially, citric acid monohydrate was dissolved in 100 mL of distilled water and stirred vigorously for 10 minutes to form a uniform solution. Subsequently, lead nitrate, zirconium oxychloride, titanium tetraisopropoxide, and finally lanthanum (III) nitrate hexahydrate were added in sequence. To facilitate the reaction, 5 mL of nitric acid (HNO_3) was introduced at the final stage. The resulting mixture was stirred continuously for one hour at room temperature to ensure a clear and homogenous complex solution.

To start the gel formation process, the temperature was progressively raised to 80°C. The gel was then dried at the same temperature. The resultant powder was first pre-calcined at 600°C for three hours after auto-combustion. To create a single-phase powder, a second heat treatment was performed for an additional three hours at about 850°C. The development of the perovskite structure was verified by X-ray diffraction (XRD). A PANalytical Xpert-Pro-Philips diffractometer operating with CuKα radiation (λ = 1.5406 Å) over a 2θ range of 10° to 90° was used to perform the XRD experiments at room temperature. Using a Seiko EXSTAR6200 TG/DTA system (Japan) and thermogravimetric analysis (TGA), the thermal behaviour of the dried gel was investigated, including its crystallization and breakdown properties during annealing. The optimized lanthanum-doped PZT (52/48) powder was then used to fabricate pellets for dielectric and ferroelectric characterization.

The PL(92.5/7.5)ZT(52/48) pellet was made by adding a certain quantity of polyvinyl alcohol (PVA) and grinding it hard to distribute it throughout the sample. A hydraulic pelletizer set to 50 kN of applied pressure was used to pelletize the powder after it had been sintered for four hours at 875°C. The PL(92.5/7.5)ZT(52/48) sample was examined microstructurally and its grain size was determined using scanning electron microscopy (SEM) (Model: FEI Quanta 3D FEG). The sintered pellet was polished to make sure both faces were flat before being coated in high-quality silver paste to act as electrodes for electrical investigation. Using a Solartron SI 1260 impedance gain-phase analyzer, the dielectric characteristics of the sintered PLZT ceramic were examined at various temperatures and frequencies.

The sample was heated steadily at a rate of 3°C per minute during the measurements, and an AC signal with an amplitude of 1 V was applied. The relative permittivity, capacitance, and loss tangent were measured at frequencies ranging from 100 Hz to 1 MHz and temperatures ranging from 25 to 600°C. A ferroelectric loop tracer from Radiant Technology was used to measure the ferroelectric hysteresis loops of the PLZT pellet in order to ascertain the coercive electric field and remnant polarization at various applied voltages.

3. Results and Discussion

3.1. Structural and morphology studies

According to X-ray diffraction (XRD), the phase formation behaviour of the calcined PL(92.5/7.5)ZT(52/48) ceramics is displayed in Fig. 1. None of the samples showed any signs of the pyrochlore phase ($A_3B_4O_{13}$), which is generally regarded as undesirable in PZT materials. Rather, a strong peak at 2θ = 31.20° proved the presence of the perovskite PZT phase. To determine the phases present, the diffraction peaks were indexed using the measured interplanar spacings (hkl) and compared with standard JCPDS data (file no. 33–0784). While doping with La2 + ions at the A-site did not appreciably impact the fundamental crystal structure of PZT, a modest shift in the peak positions suggested a slight modification in the lattice characteristics.The presence of nanocrystalline particles was shown by the XRD peaks' broadness. The average crystallite size of the lanthanum-doped PZT was determined to be roughly 33.4 nm using Scherrer's equation ($t = 0.9\lambda/\beta\cos\theta$).

Thermogravimetric analysis (TGA) and differential thermal analysis (DTA) were used to heat the PL(92.5/7.5)ZT(52/48) powder at a rate of 20°C/min in a helium environment, as illustrated in Fig. 2. Between 180 and 250°C, the TGA curve indicates a weight loss of roughly 15%, which is probably caused by the sample losing moisture. Citric acid and other organic molecules break down between 300 and 390°C, resulting in an additional weight decrease of about 20%. Three separate exothermic peaks may be seen on the DTA curve at 176, 345, and 460°C. The combustion of titanium (IV) isopropoxide, citric acid, and other organic leftovers within the PLZT polymerized gel is responsible for the first peak. The second peak, which happens between 300 and 390°C, is caused by the combustion of residual carbonaceous material, nitrate release, and organic molecule breakdown. A 5% weight loss and the beginning of the material's crystallization are indicated by the third, wider peak, which is located at about 460°C.

Scanning electron microscopy was used to analyze the PLZT pellet's surface morphology (SEM). The average particle size, as shown in the SEM image (Fig. 3), is roughly 0.3 μm. During pellet creation, which included adding PVA and sintering for four hours at 875°C, particle agglomeration is probably the cause of the observed increase in particle size when compared to the initial powder [20]. The presence of lanthanum is further confirmed by energy-dispersive X-ray (EDX) analysis (Fig. 3c), which shows a noticeable lanthanum peak close to the particles.

3.2. Dielectric properties

Using the AC technique of complex impedance spectroscopy (CIS), dielectric experiments were performed to investigate the response of the PL(92.5/7.5)ZT(52/48) pellet to an applied AC voltage (1 V) as a function of temperature and frequency. This method allows for an accurate depiction of the material properties by differentiating between the real and imaginary components of electrical characteristics. The PL(92.5/7.5)ZT(52/48) pellet's loss tangent (tan δ) is shown in Fig. 4(b) as a function of temperature over a frequency range of 100 Hz to 1 MHz. The highest dielectric loss over the temperature range under study is around 74 (± 1%), and the loss tangent increases with frequency. The relative permittivity (εr) changes with frequency and temperature, as seen in Fig. 4(a). At all temperatures, the relative permittivity decreases with increasing frequency, achieving a peak value (ε_{rmax}) of about 27,780 (± 1%) at 600°C. The pronounced transition peaks suggest that lanthanum doping induces relaxor-like behaviour in the ceramics. The introduction of trivalent La^{3+} ions generate A-site vacancies, which, combined with thermal treatment of the fine-grained sample, contributes to this effect. The dielectric permittivity shows significant frequency dependence, declining as frequency increases across all temperatures, due to the inability of dipoles to respond quickly to the applied field changes. This results in lower relative permittivity values at higher frequencies. The low ε_r values observed are intrinsic and not influenced by external Maxwell-Wagner polarization effects, with grain size reduction from doping being the primary cause of this behaviour [22, 23].

3.3. Impedance Analysis

The PL(92.5/7.5)ZT(52/48) ceramic's complex impedance spectrum (Nyquist plot), which was measured at different temperatures throughout a frequency range of 100 Hz to 1 MHz, is shown in Fig. 5. The impact on the impedance behaviour of the material intensifies with increasing temperature. Dipolar relaxation mechanisms in the material are responsible for the semicircular arcs seen in the high-frequency region [24]. As shown in the Fig. 5 inset, each semicircle in the impedance plot denotes a parallel RC circuit element. The intersection of these arcs with the real axis provides information about the resistance, capacitance, and grain boundary characteristics of the sample. The arcs get increasingly semicircular as the temperature increases, and their centres move in the direction of the complicated plane plot's origin. This change suggests that the sample's resistive behaviour has decreased, maybe as a result of grain boundary conduction becoming more pronounced with temperature [25].

Figure 6 displays the frequency-dependent imaginary component of impedance (Z") of PLZT ceramics, which exhibits many peaks at elevated temperatures. As the temperature rises, these peaks broaden, decrease in height, and shift to higher frequencies. This implies that bulk resistance is dropping with temperature and that the material is going through a thermally induced dielectric relaxation process. Because these peaks occur above the measuring frequency range or because the material has weak current dissipation, they are not visible at low temperatures (not pictured). The peaks' apparent expansion with increasing temperature suggests that the material may be undergoing a temperature-dependent relaxing process. These dispersion curves tend to mix together at higher frequencies because space charge polarization is less common at higher frequencies than at lower ones.

3.4. DC conductivity studies

Figure 7 shows the variation of DC conductivity with temperature for PL(92.5/7.5)ZT(52/48) ceramics within the range of 425–600°C. The activation energy (E_a) of the sample was calculated using the relation:

$\sigma_{ac} = \sigma_o exp(-E_a/k_B T)$

where T is the temperature in Kelvin, k_B is the Boltzmann constant, and σ_0 is the pre-exponential factor. The activation energy determined for the PL(92.5/7.5)ZT(52/48) sample was found to be 0.169 eV. DC conductivity's temperature-dependent behaviour indicates that a thermally triggered mechanism is responsible for electrical conduction in the material. The heat production of charge carriers as oxygen vacancies in the perovskite ferroelectric structure ionize is probably the cause of this. This implies that oxygen vacancies are the cause of charge carrier conduction at high temperatures. The formation of micron-sized domains reduces the coupling between BO6 octahedral sites, resulting in a lower activation energy for the dopant.

Trivalent lanthanum doping reduces the size of these micropolar regions, which are created by doping [24]. Consequently, the long-range ferroelectric behaviour of the weak coupling decreases as the temperature rises, resulting in a drop in both activation energy and conductivity. No comparisons with existing experimental results were possible due to the lack of available data for the specific PL(92.5/7.5)ZT(52/48) composition near the morphotropic phase boundary (MPB).

3.5. Ferroelectric studies

At room temperature, ferroelectric hysteresis loop measurements were performed with voltages between 500 and 4000 V at a frequency of 250 Hz. Figure 8 shows the loops that resulted. At all applied voltages, coercive field and remnant polarization were seen in the hysteresis loops, and both increased when the voltage was increased from 0.5 kV to 4.0 kV. The values of saturation polarization (Ps), remnant polarization (Pr), and coercive electric field (Ec) that were taken from these loops for every voltage level are listed in Table 1. The sample showed a maximum remnant polarization of 3.04 μC/cm² and a coercive field of 6.12 kV/cm at the maximum applied voltage of 4.0 kV. Lanthanum doping tends to increase the likelihood of short circuits in PZT by creating more voids and reducing grain size under high voltage conditions. The enhanced saturation and remnant polarization indicate strong ferroelectric behaviour. Compared to the undoped PZT, the lanthanum-doped ceramics demonstrate higher saturation and remnant polarization, consistent with findings from our earlier study on both undoped and La-doped PZT (52/48) [15].

Table 1
Saturation Polarization (P_s), remnant polarization (P_r) and coercive field (E_c) determined from the measured hysteresis loop of La doped PZT nanoceramics.

Applied Voltage (kV)	**Remnant Polarization (P_r) ($\mu C/cm^2$)**	**Saturated Polarization (P_s) ($\mu C/cm^2$)**	**Coercive field (E_c) (kV/cm)**
0.5	Negligible	0.43	Negligible
1.0	0.14	1.08	0.65
1.5	0.40	2.00	1.55
2.0	0.83	3.10	2.56
2.5	1.36	4.31	3.71
3.0	2.00	5.55	4.72
3.5	2.66	6.73	5.65
4.0	3.04	7.24	6.12

4. Conclusion

Ferroelectric PL(92.5/7.5)ZT(52/48) powder was successfully synthesized using the sol-gel technique. X-ray diffraction (XRD) analysis confirmed that the ceramic powder exhibited a single-phase tetragonal perovskite (ABO_3) structure. The crystallization temperature of the PL(92.5/7.5)ZT(52/48) powder was determined through thermogravimetric and differential thermal analyses (TG/DTA). SEM imaging revealed that the pelletization process caused surface agglomeration, resulting in a non-uniform particle distribution. Dielectric experiments were conducted between 25°C and 600°C in temperature and between 100 Hz and 1 MHz in frequency. The electrical conductivity's temperature dependency was investigated using impedance spectroscopy. The impedance measurements showed that both the relative permittivity and the loss tangent dropped with increasing frequency. The activation energy was determined to be 0.169 eV using the Arrhenius plot of DC conductivity versus the inverse of absolute temperature. Ferroelectric hysteresis loop experiments at room temperature with an applied voltage of 4 kV revealed a remnant polarization (Pr) of 3.04 μC/cm² and a coercive electric field (Ec) of 6.12 kV/cm.

Declarations

Compliance with Ethical Standards

I ensure objectivity and transparency in research and accepted principles of ethical and professional conduct have been followed.

Funding

This research did not receive any specific grant from funding agencies in the public, commercial, or not-for-profit sectors.

Competing Interest

The authors declare that they have no known competing financial interests or personal relationships that could have appeared to influence the work reported in this paper.

Research Data Policy and Data availability statement

Any data that support the findings of this study are included within the article.

Author's Contribution

Author 1:

Writing - Original Draft

Preparation, creation and presentation of the published work, specifically writing the initial draft (including substantive translation)

Author 2:

Writing - Review & Editing

Preparation, creation and presentation of the published work by those from the original research group, specifically critical review, commentary or revision – including pre-or post-publication stages

References

1. Sagar E, Shirsath C, Cazorla T, Lu L, Zhang YY, Tay X, Lou Y, Liu S, Li D, Wang (2020) Nano Lett 20(2):1262–1271. https://pubs.acs.org/doi/abs/ 10.1021/acs.nanolett.9b04727
2. Lee W, Han H, Lotnyk A, Schubert MA, Senz S, Alexe M, Hesse D, Balk S, Gosele U (2008) Nat Nanotechnol 3:402–407. https://doi.org/10.1038/nnano.2008.161
3. Sagar E, Shirsath M, Hussein N, Assadi J, Zhang N, Kumar AS, Gaikwad J, Yang HE, Maynard-Casely YY, Tay J, Du H, Wang Y, Yao Z, Chen J, Zhang S, Zhang S, Li, Wang D (2022) ACS Nano 16(9):15413–15424. https://pubs.acs.org/doi/abs/ 10.1021/acsnano.2c07215
4. Tahani M, Alfareed Y, Slimani MA, Almessiere, Sagar E, Shirsath M, Hassan M, Nawaz FA, Khan, Ebtesam A, Al-Suhaimi A, Baykal (2022) Ceram Int 48(10):14640–14651. https://doi.org/10.1016/j.ceramint.2022.01.358
5. Jaffe B, Cook WR, Jaffe H, Ceramics P (1971) Academic, New York, pp. 135–171

6. Noheda B, Cox DE, Shirane G, Gonzalo JA, Cross LE, Park S-E (1999) Appl Phys Lett 74:2059–2062. https://doi.org/10.1063/1.123756
7. Raju K, Venugopal Reddy P (2010) Curr Appl Phys 10:31–35. https://doi.org/10.1016/j.cap.2009.04.017
8. Nowotny J, Rekas M (1994) Ceram. Int. 20, 265–275. https://doi.org/10.1016/0272-8842(94)90061-2
9. Yassine Slimani SE, Shirsath E, Hannachi MA, Almessiere MM, Aouna NE, Aldossary (2021) Ghulam Yasin, Abdulhadi Baykal, Bekir Ozçelik, Ismail Ercan. J Am Ceram Soc 104:5648–5658. https://doi.org/10.1111/jace.17931
10. Kowalski K, Ijjaali M, Bak T, Dupre B, Nowotny J, Rekas M, Sorrell CC, Zhao Y (2001) J Phys Chem Solids 62:531–535. https://doi.org/10.1016/S0022-3697(00)00211-0
11. Yuan Y, Zhang SR, Zhou XH (2009) J Mater Sci 44:3751–3757. https://doi.org/10.1007/s10853-009-3502-z
12. Li H, Kang J, Guo F, Qu Y, Yang D (2013) Ceram Int 39:7589–7593. https://doi.org/10.1016/j.ceramint.2013.03.013
13. Mostafa Bourim EI, Kim H-Y, Yang J-S, Yang J-W, Woo K-S, Song J-H, Yun S-K (2009) Sens Actuators A 155:290–298. https://www.sciencedirect.com/science/article/abs/pii/S0924424709003951
14. Guerra JDS, Garcia JE, Ochoa DA, Pelaiz-Barranco A, Garcia-Zaldivar O, Calderon-Pinar F (2012) J Mater Sci 47:5715–5720. https://link.springer.com/article/ 10.1007/s10853-012-6461-8
15. Prabu M, Shameem Banu IB, Gobalakrishnan S, Chavali M (2013) J Alloys Comp 551:200–207. https://www.sciencedirect.com/science/article/abs/pii/S0925838812016891
16. Bouayad K, Sayouri S, Lamcharfil T, Ezzejari M, Mezzane D, Hajji L, Ghazouali AEI, Filalil M, Dieudonne P, Rhouta M (2005) Phys A 358:175–183. https://www.sciencedirect.com/science/article/abs/pii/S0378437105005947
17. Silva PS Jr., Florencio O, Botero ER, Eiras JA, Garcia D (2009) Mater Sci Engg 521:224–227. https://www.sciencedirect.com/science/article/abs/pii/S0921509309002202
18. Garcia-Zaldivar O, Pelaiz-Barranco A, Guerra JDS, Mendoza ME, Calderon-Pinar F, Hall DA (2011) Phys B 406:1622–1626. https://www.sciencedirect.com/science/article/abs/pii/S0921452611001232
19. Sagar E, Shirsath D, Wang SS, Jadhav ML, Mane S, Li (2018) Handbook of Sol-Gel Science and Technology. Springer Cham, pp 695–735
20. Prabu M, Shameem Banu IB, Kannan D, Gobalakrishnan S, Chavali M (2013) J Mater Sci: Mater Electron 24:1556–1561. https://link.springer.com/article/ 10.1007/s10854-012-0972-6
21. Prabu M, Shameem Banu IB, Gobalakrishnan S, Chavali M (2013) Adv Sci Eng Med 5:496–499. https://doi.org/10.1166/asem.2013.1280
22. Rongli Gao Z, Wang G, Chen X, Deng W, Cai (2018) Ceram Int 44. https://doi.org/10.1016/j.ceramint.2018.08.234. S84-S87

23. Rongli Gao X, Qin Q, Zhang Z, Xu Z, Wang C, Fu G, Chen X, Deng W, Cai (2019) J Alloys Comp 795:501–512. https://doi.org/10.1016/j.jallcom.2019.05.013
24. Lin GC, Zhang JX (2001) 256 (1), 69–80. https://www.tandfonline.com/doi/abs/10.1080/00150190108015974
25. Dai X, DiGiovanni A, Viehland D (1993) J Appl Phys 74:3399–3405. https://doi.org/10.1063/1.354567

Figures

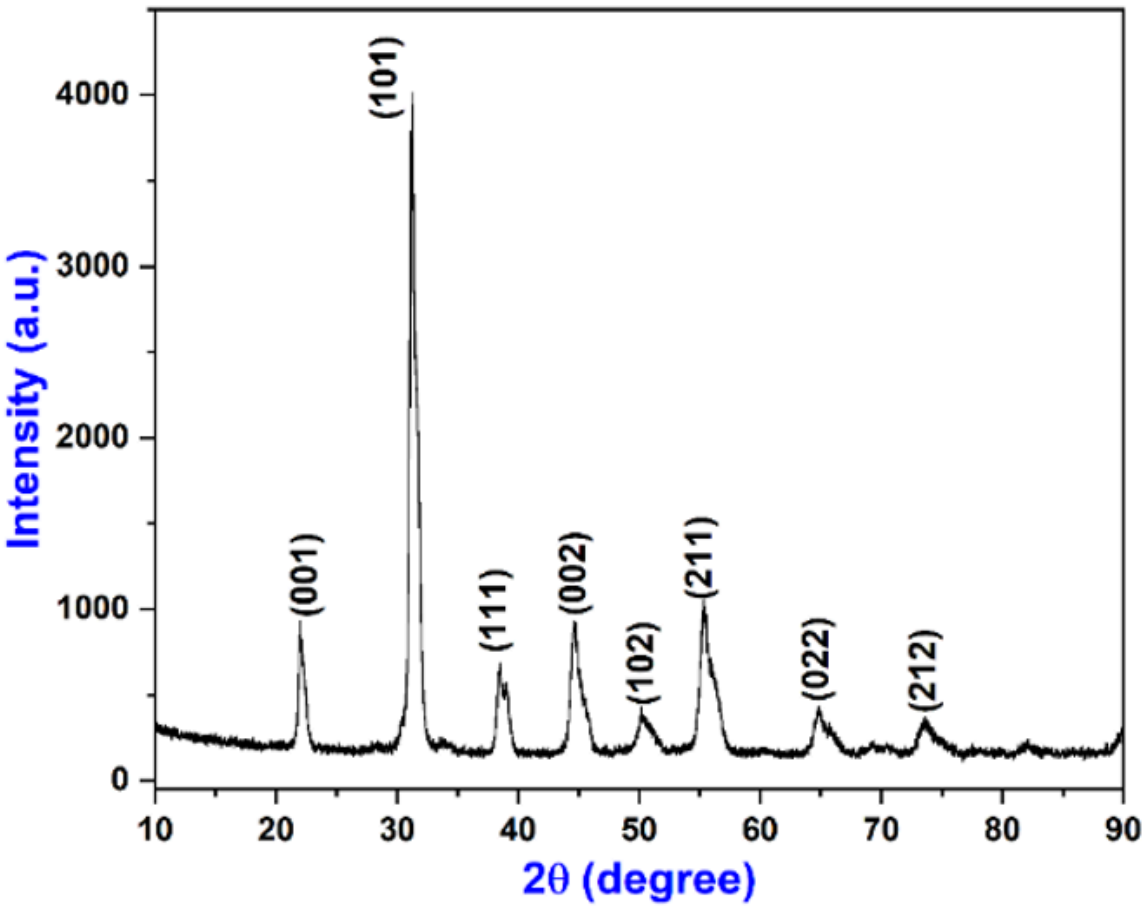


Figure 1

XRD pattern of the PL(92.5/7.5)ZT(52/48)nanoceramics calcined at 850 °C for 3 hrs and its showing high crystallinity of sample.

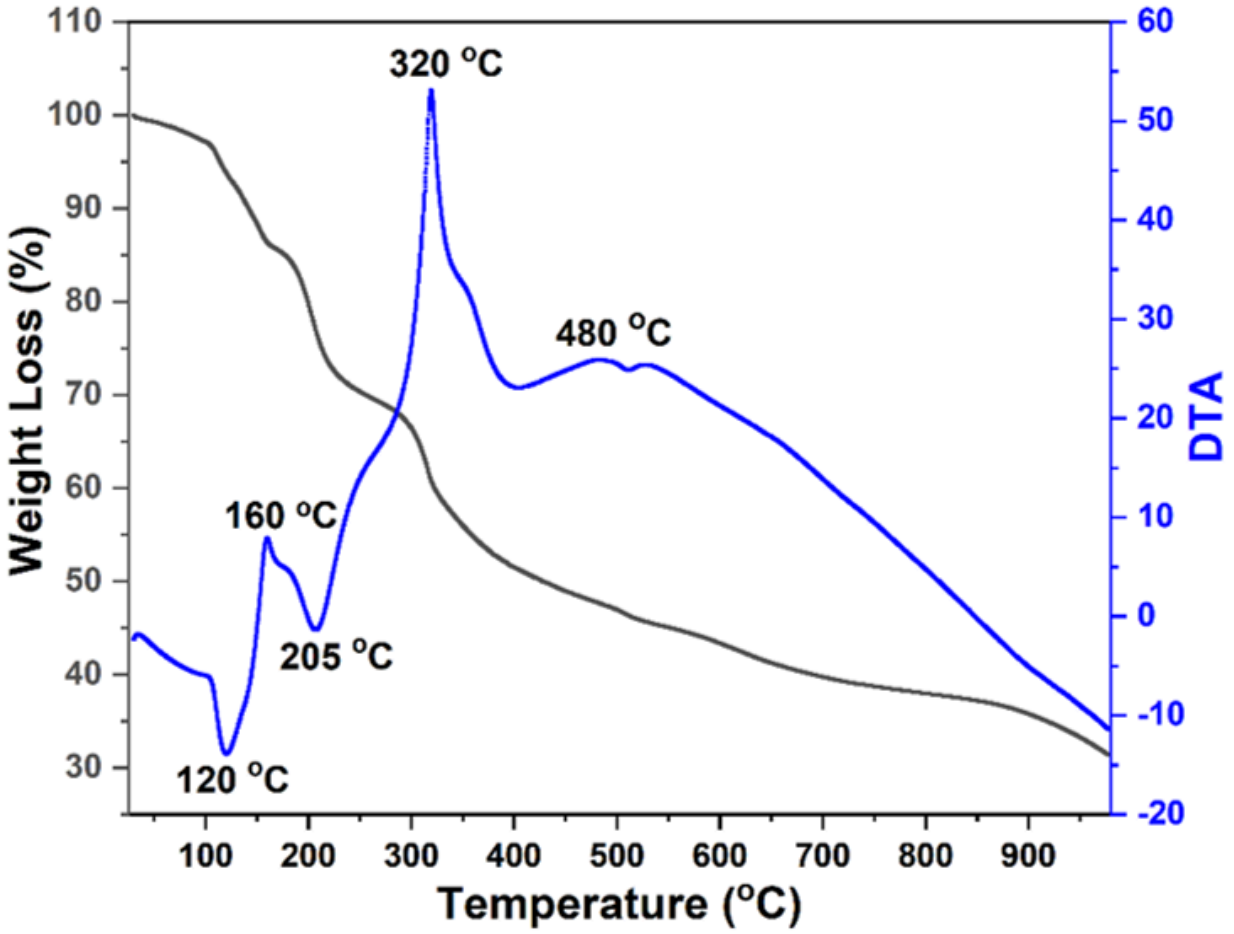


Figure 2

Thermogravimetric and differential thermal analysis of lanthanum doped PZT ceramics for the temperature range of room temperature to 1000 °C.

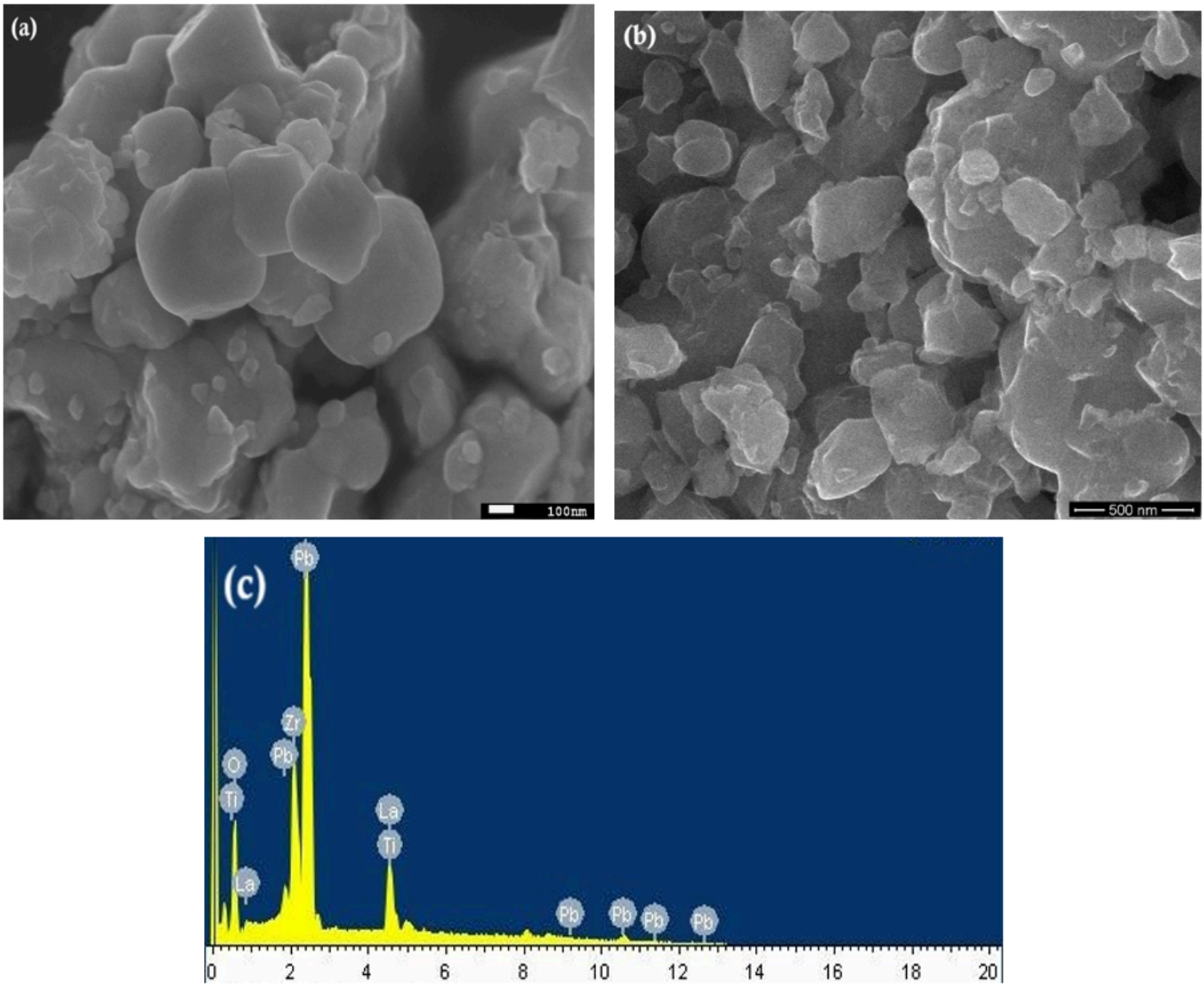


Figure 3

The SEM image of lanthanum doped PZT (52/48) (a) powder calcined at 850 °C for 3 hrs and (b) pellet sintered at 875 °C for 4 hrs (c) EDAX measurements.

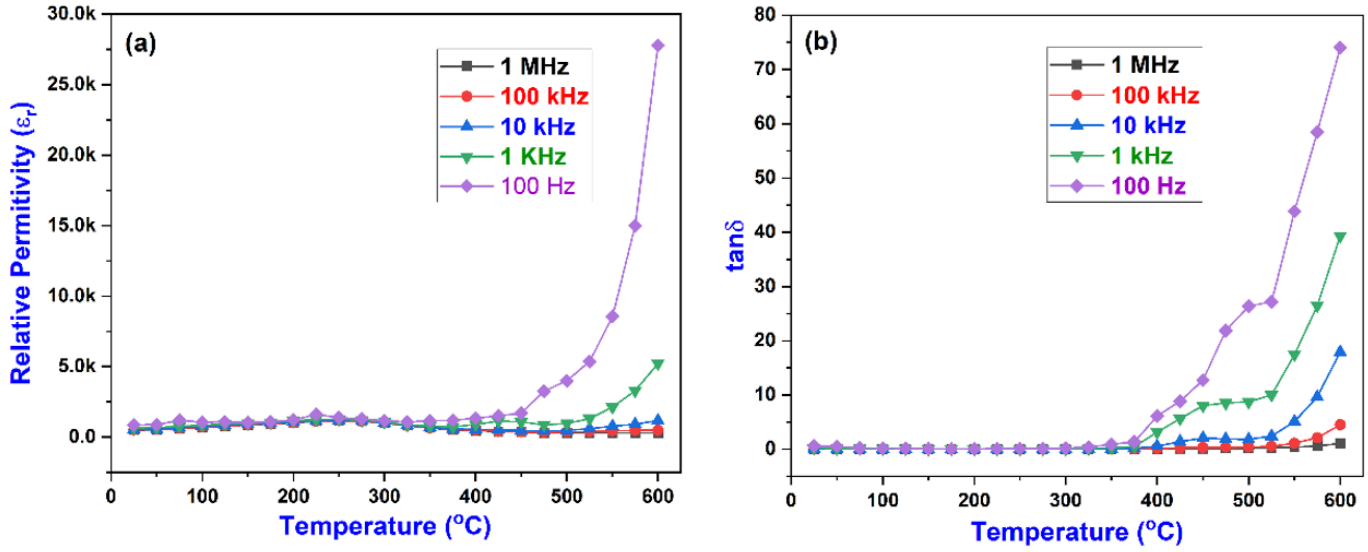


Figure 4

(a) Relative permittivity and (b) Dielectric loss of PL(92.5/7.5)ZT(52/48) nanoceramics.

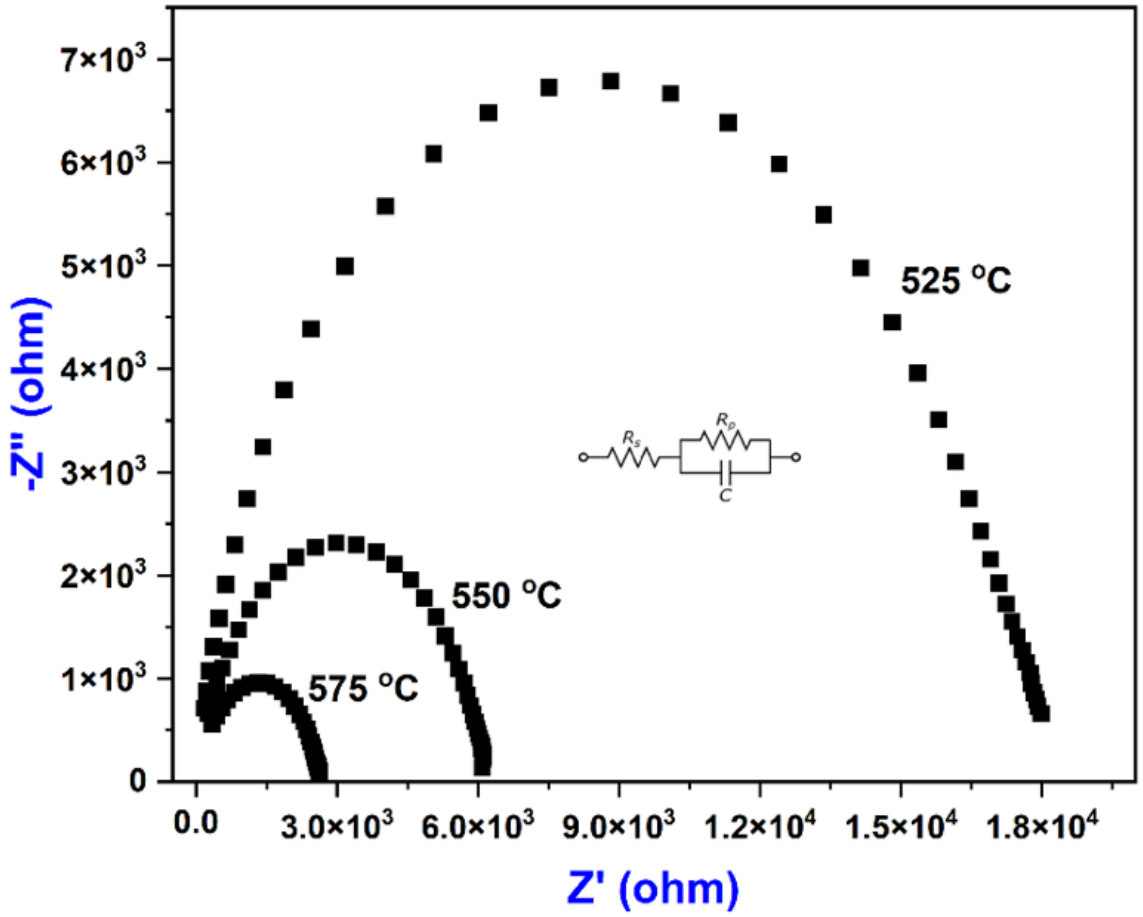


Figure 5

Complex impedance spectrum as a function of frequency for PL(92.5/7.5)ZT(52/48) nanoceramic at various temperature.

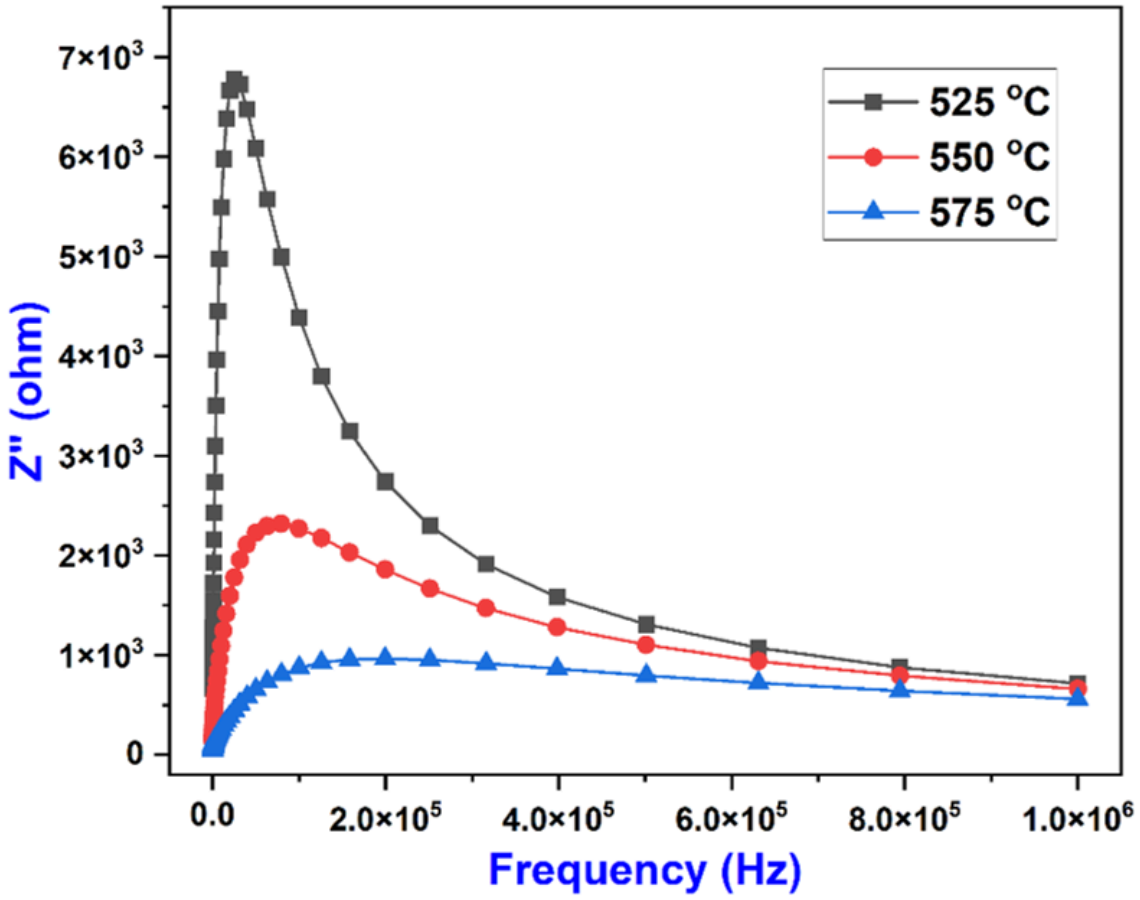


Figure 6

Loss spectrum as a function of frequency for PLZT ceramic at various temperature.

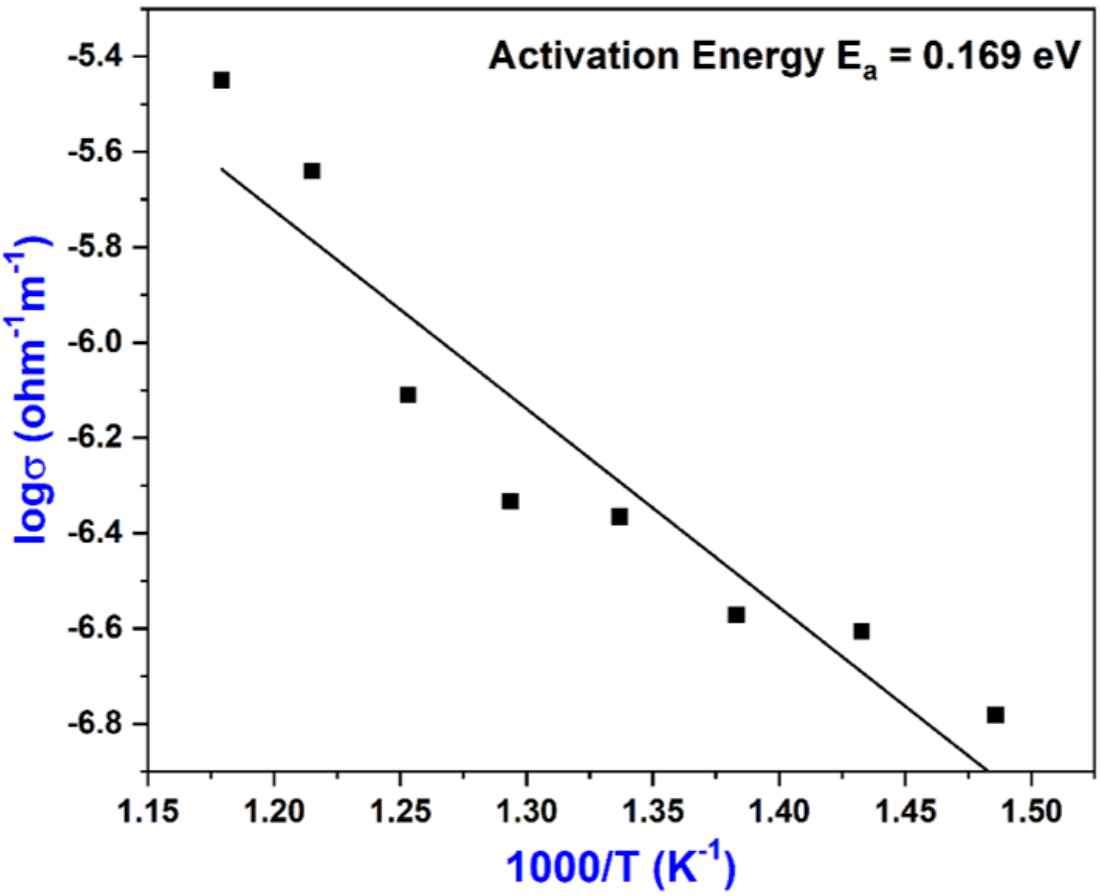


Figure 7

Activation energy (E_a) of Lanthanum-doped PZT ceramics derived by fitting to the Arrhenius equation.

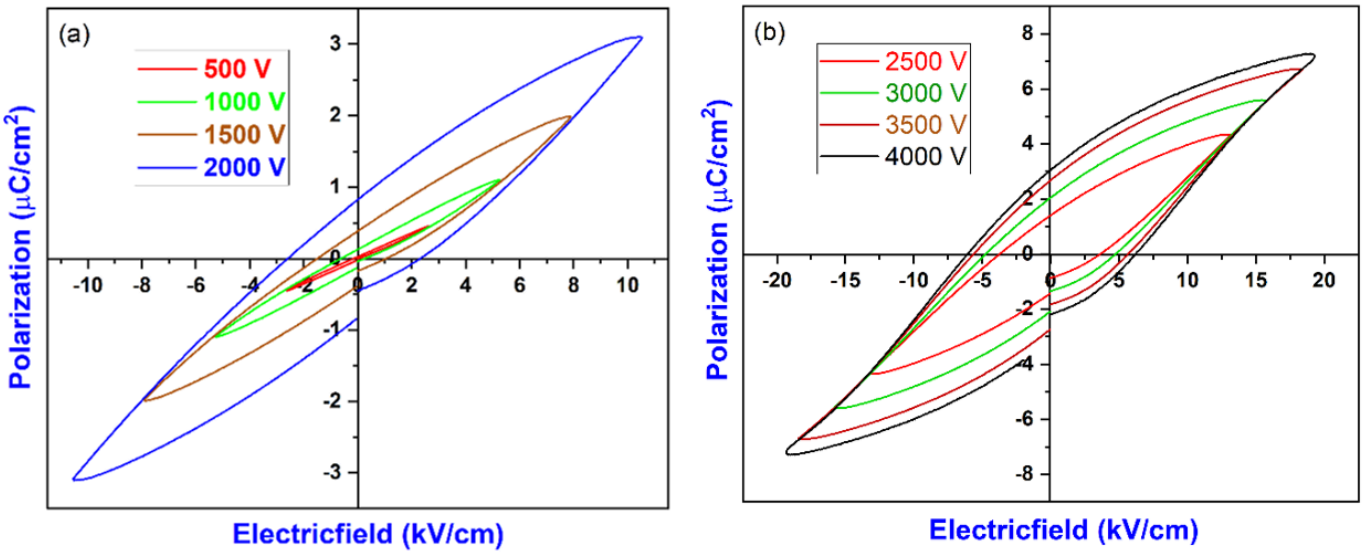


Figure 8

Ferroelectric hysteresis loops obtained for La doped PZT with applied voltages ranging from 500 V to 4000 V, measured at room temperature at a frequency of 250 Hz.